ISSN 0001-4338, Izvestiya, Atmospheric and Oceanic Physics, 2022, Vol. 58, No. 12, pp. 1599–1609. © Pleiades Publishing, Ltd., 2022.
Russian Text © The Author(s), 2022, published in Issledovanie Zemli iz Kosmosa, 2022, No. 4, pp. 53–65.

USE OF SPACE INFORMATION ABOUT THE EARTH ENVIRONMENTAL STUDIES BASED ON SPACE DATA

On The Long-Term Stability of the Norilsk TPP-3 Fuel Tanks Dynamics According to Sentinel-1 SAR Data

A. I. Zakharov[a], * and L. N. Zakharova[a]

[a] *Kotelnikov Institute of Radioengineering and Electronics, Russian Academy of Sciences, Fryazino Branch, Fryazino, Russia*

**e-mail: aizakhar@ire.rssi.ru*

Received October 29, 2021

Abstract—The results of the interferometric processing and analysis of European spaceborne synthetic aperture radar (SAR) Sentinel-1 acquired over the territory of Norilsk thermal power plant TPP-3 between July 2017 and August 2020 are presented. Twelve-day differential interferograms allow the estimation of the stability of the position of all TPP-3 oil reservoirs with respect to reference known stable targets. The strong distorting influence of meteorological precipitation, as well as of the freeze–thaw processes of snow cover on the TPP-3 territory, on the quality of interferometric phase measurements is noted. It is found that on all of the twelve-day interferometric observation intervals from July 2019 to August 2020 made in warm seasons, the relative position of all four reservoirs and the adjacent territory is stable within the accuracy of about 1.3 mm. According to observations of the reservoirs between July 2017 and August 2020 using summer interferograms with a one-year interval between image acquisitions, the long-term stability of the position is about 4 mm. We can conclude that the reservoir damage was not caused by areal displacements of the scattering surfaces in the study area, supposedly due to the melting of permafrost in the area of the reservoirs.

Keywords: Norilsk, fuel storage tank, synthetic aperture radar interferometry, Sentinel-1, corner reflector, surface dynamics

DOI: 10.1134/S0001433822120271

INTRODUCTION

The spill of oil products on May 29, 2020 at the fuel storage facility of TPP-3 in the city of Norilsk, in terms of the degree of environmental impact became an environmental disaster on a federal scale. As a result of depressurization of one of the fuel storage tanks, 21 000 tons of diesel fuel leaked. One of the main possible explanations of the cause of the accident, voiced by the management of the Norilsk Nickel metallurgical and mining company, was the thawing of frozen ground due to abnormally warm weather, which may have caused damage to the supports on which the platform with the tank stood.

For monitoring areas of emergency situations, as well as retrospective monitoring using archival data, it is effective to use space methods (Bondur, 2010) in combination with methods for processing aerospace images (Bondur and Starchenkov, 2001). The problems of remote measurement of surface displacements of different nature can be successfully solved using the differential interferometry method (Bamler and Hartl, 1998), (Zakharova and Zakharov, 2019). Radar interferometry in the scheme of land-cover surveys from repeated carrier orbits as a means of detecting small-scale surface displacements during the time between surveys is used in many applications of Earth remote sensing methods. As examples, close in subject matter and processing methods to the current study, we can mention works on the observation of cyclic displacements of peat soils in the Selenga River delta due to frost heaving in winter and subsidence due to drying in summer (Dagurov et al., 2016), observation of centimeter shifts of the surfaces of a landslide slope on the banks of the Bureya River (Zakharova and Zakharov, 2019), temperature deformations of railway bridge spans (Zakharova and Zakharov, 2018), and observation of landslide processes using artificial corner reflectors under conditions of strong temporal decorrelation (Zakharov et al., 2018).

There is a technology for monitoring the dynamics of the underlying cover, specially designed for use in conditions of high temporal decorrelation of the natural cover. It is based on the use of a set of radar images processed using the permanent scatterers method, denoted by the abbreviation PS, i.e., Permanent Scatterers (Ferretti et al., 1999, 2000; Colesanti et al., 2003a, 2003b), and variants of the development of this method: SQUEESAR (Ferretti et al., 2011), STAMPS (Hooper et al., 2004), SBAS small baseline method (Berardino et al., 2002), etc. For their correct operation, it is necessary to have "permanent scatterers," i.e., objects that give a stable echo signal throughout the entire series of surveys. Having an insufficient

number of such scatterers, or their insufficient stability over a long series of surveys, are potential limitations of this group of methods. Preliminary data-processing and analysis has shown that a noticeable temporal decorrelation even on well-backscattering infrastructure objects of the thermal power plant and the metallurgical plant will not allow us to obtain reliable results when using PS methods, so the current study is based on the calculation and analysis of the time series of standard differential interferograms (DInSAR).

USED DATA

The technology of radar interferometry involves observations from close orbits of the carrier of radar equipment. European Space Agency Sentinel-1 Synthetic Aperture Satellite Radars (SAR), performing regular surveys from repetitive orbits at intervals of 12 days in the C-band (wavelength $\lambda = 5.6$ cm), are one of the most suitable data sources for the purposes of this work. The analysis of the Copernicus archive (see https://scihub.copernicus.eu/dhus/#/home) has revealed images of the territory of the TPP-3 by the Sentinel-1B satellite from October 2016 to the present, suitable for interferometric processing. The surveys were carried out on the descending part of the orbit in the right-looking geometry with an incidence angle of 41°. On June 9, 2020, a few days after the disaster, an additional image was taken from the Sentinel-1A satellite in the same observation geometry, which made it possible to form two additional interferometric pairs with an interval between observations of half the normal length, i.e., six days. Thus, we used interferometric pairs with different intervals between surveys: from six days to one year.

The used Sentinel-1 Data, with Single Look Complex processing level, were obtained in the IW wide-swath interferometric survey mode using the method of progressive scanning of the surveyed area with an antenna beam in the azimuthal direction (terrain observation with progressive scans, TOPS (Torres et al., 2012)). A wide swath was provided by successive illumination of elementary frames with switching of the viewing angle in the elevation plane, and periodic repetition of the scanning sequence from a moving carrier ensured an increase in the survey swath. Each pixel of the image is represented by complex signal samples (in-phase and quadrature components). The distance between pixels along the slant range is 2.3 m and the distance between the pixels of adjacent rows in the azimuth direction is 14.1 m.

CHARACTERISTICS OF OBSERVATION OBJECTS IN THE SURVEY AREA

The climate of the region is characterized by subzero average annual air temperature, long winters with severe frosts and snowstorms, very short rainy and cold summers, and frequent and abrupt weather changes. The polar day lasts from May 20 to July 24; the minimum average precipitation of the three summer months occurs in July (32 mm) and the maximum in August (52 mm). A stable snow cover forms in the first half of October, disappearing around mid-May. The dominant winds of the southern quarter in winter are the cause of the transfer of large masses of snow, the formation of deep snowdrifts, and the formation of sastrugi on the snow surface. This region is characterized by continuous permafrost. Tundra gley soils are the most typical; marsh and alluvial soils are also found (Vasil'evskaya, 1980).

The TPP-3 is adjacent to B.I. Kolesnikov Metallurgical Plant from the southwest, constituting with it a single industrial zone on the edge of the Nadezhda Plateau. The territory of the vicinity of the TPP-3 from a Google Earth image is shown in Fig. 1. The inset at the top right shows an enlarged fragment of the image with a line of fuel tanks oriented diagonally. The tanks are numbered from bottom to top, from tank No. 2 to tank No. 5 (you can also distinguish a round trace from the previously dismantled tank No. 1). The long arrow at the right edge 1 shows the direction of flight of the Sentinel-1 satellite; the wide arrows show the radar looking direction (to the right in the direction of the carrier). Since the survey is carried out approximately from the east direction, the western walls of the tanks and a small part of the industrial site adjacent to them are in the radio shadow. Accordingly, that side of the emergency tank No. 5, where the wall ruptured and fuel leaked (the short white arrow in the inset in Fig. 1) is not directly visible on the Sentinel-1 images.

The fuel tanks are cylindrical structures with a diameter of 45 m, the centers of which are located at a distance of 75–78 m from each other. The slope of the cone-shaped roofs of the tanks does not exceed 20°. The radar images of such objects, with surfaces that are smooth on the scale of the radar signal wavelength, differ from the usual optical images. The dominant mechanism of radio-wave interaction with the smooth metal surface of the tank structure is mirror reflection. As a result, the signal scattered by the roof, S_R, does not return to the radar in the Sentinel-1 survey geometry (Fig. 2) and therefore is not registered by the receiving antenna.

The signal scattered by the walls of the tanks and the adjacent surface of the site consists of two components: double bounce scattering D and single scattering S. The side wall of the tank forms a dihedral angle with the surface of the industrial site, due to which, after successive specular reflection by the AO wall and the surface of the OB site, the signal returns to the radar (see Fig. 2, beams D_1 and D_2 in the diagram on the right). A feature of the signal scattered by a dihedral corner is the equality of the path length for all rays incident on the edges, as a result of which a tank with a height of about 20 m looks like a bright point target on the radar image with a resolution of 2.3 m at a slant

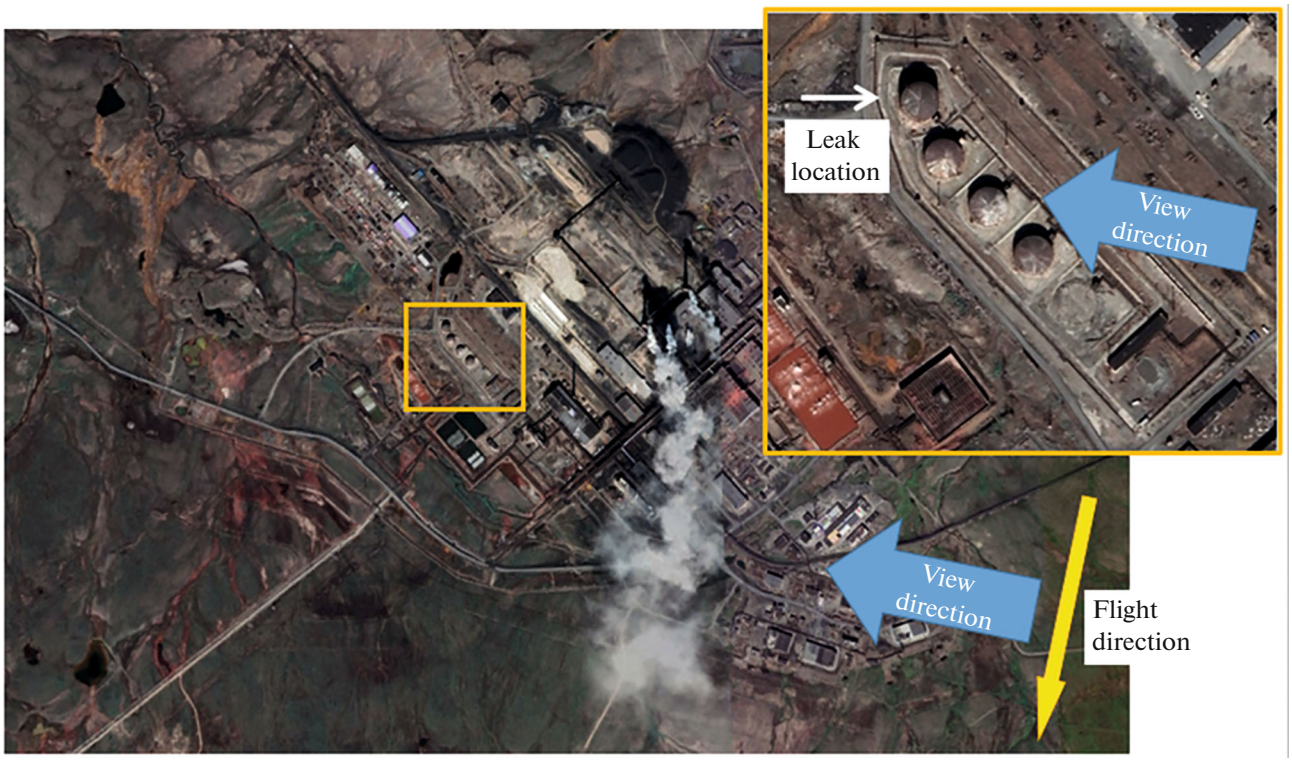

Fig. 1. Image of the TPP-3 territory and the survey geometry of the Sentinel-1 SAR on a descending orbit.

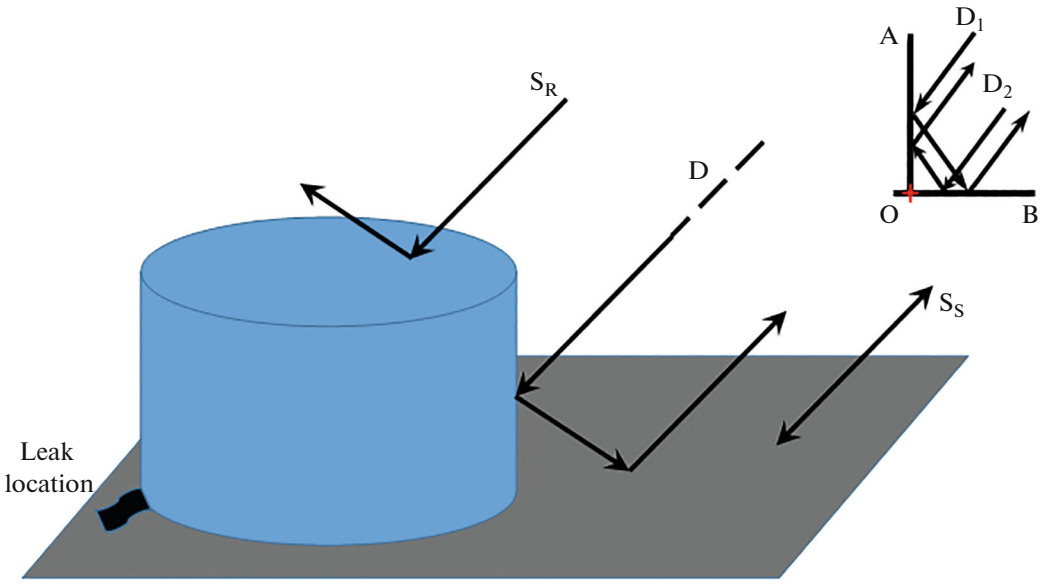

Fig. 2. Interaction of radio waves with the reservoir structure and industrial site.

range, located at a position corresponding to the height of the corner, i.e., point O. Small-scale displacements of the corner faces lead to a displacement of the position of the vertex O and, accordingly, a change in the distance to the radar. In contrast to the mirror-reflected roof and the signal S_R, which does not affect the formation of the radar image in any way, the backscatter signal from the adjacent rough surface of the industrial site S_S is recorded by the radar, which makes it possible to observe its dynamics even in the absence of a double bounce scattering by the side surface of the tank.

Although the corner reflector has a wide backscatter pattern, the deviation of its faces from strict mutual orthogonality leads to the splitting of the main lobe of the pattern into two narrow lobes, the direction of which is slightly different from the direction to the radar (Kobak, 1975). As a result, fluctuations in the level of the scattered signal are possible when the angle of observation of the object by the radar changes. The least stable part of the dihedral angle design is the uneven surface of the industrial site (line OB in Fig. 2). As a result of soil moisture after rain, the signal scattering conditions along the OB line may change, which may cause a change in the level and direction of the scattered signal, as well as a shift in the position of the top O of the dihedral angle. Most often, on the studied radar images of the TPP-3, a decrease in the level of backscatter was noted up to its complete disappearance at tank No. 3 after rains that fell in the period up to 3–5 days before observations (imaging in the warm season with the dates July 8, 2018, July 20, 2018, and September 9, 2019). Another reason for the changes in the scattering conditions for signals D_1, D_2, and S_S is the formation of snow cover on the surface adjacent to the reservoir in the cold season. In (Zakharov and Zakharova, 2017), using the analysis of signals scattered by power-line pylons on a snowy plain as an example, it is shown that, for example, a uniform fresh snow cover 4 cm thick with a snow density of 0.25 leads to an increase in the electrical length of the signal path from the radar to the effective phase scattering center by a value on the order of 1 cm. Such additives can be incorrectly interpreted as displacements or subsidence of the scattering surface. In addition, uneven snow or snow/ice cover of the site along the OB line can cause visible non-orthogonality of the edges and a corresponding decrease in the backscatter level. Probably for this reason, a noticeable decrease in the level of backscatter by tank No. 3 was observed, for example, in the conditions of a snowy soil surface on the survey days of October 24, 2018, December 6, 2019, February 28, 2020, and March 11, 2020. A drop in the level of the signal backscattered by tank No. 5 was noted on the survey days of November 10, 2017, November 5, 2018, November 17, 2018, November 29, 2018, May 28, 2019, and October 19, 2019.

METHODS AND FIRST RESULTS OF INTERFEROMETRIC PROCESSING

The method of radar interferometry is based on the use of information about the phase difference of radar echo signals registered by the radar system at two close points in space, for which the condition of mutual coherence of signals is satisfied. In this case, the phase difference of the signals depends on the difference in distances to the target and carries information about the surface relief, and in the two-pass version also about changes in the conditions for the signal to reach the target during the time between surveys (Rosen et al., 2000; Zakharov et al., 2015).

An interferogram is an image consisting of the phase difference of the signals $\Delta\varphi = \varphi_1 - \varphi_2$, obtained as a result of element-by-element complex multiplication of signal samples U_1 and U_2, scattered by the same surface element, but received at two points that differ in location in space. The expression for the complex interferogram in the two-pass scheme is as follows:

$$U_1 U_2^* = u_1 u_2 \exp\left(j\left(\varphi_1 - \varphi_2\right)\right) = u_1 u_2 \exp\left(\frac{-j4\pi\Delta r}{\lambda}\right), \quad (1)$$

where u_1 and u_2 are the signal amplitudes, Δr is the difference in distances from the survey points to the selected surface element, and λ is the wavelength.

The accuracy of measurements of the phase difference on the interferogram is determined by the coherence of the radar signals scattered by the extended surface. Interferometric coherence characterizes the measurement errors of the phase difference and, accordingly, the relative interpixel accuracy of measurement of the heights of the relief and the displacements of the underlying surface [15]. The degree of signal coherence can be estimated directly from radar data; it is determined by the following expression:

$$\gamma = \frac{E\left\{U_1 U_2^*\right\}}{\sqrt{E\left\{\left|U_1\right|^2\right\} E\left\{\left|U_2\right|^2\right\}}}, \quad (2)$$

where $E\{\ \}$ is the operation of taking the mathematical expectation for some spatial ensemble of samples centered on the current element/pixel of the image. The analytical expression for the dependence of the dispersion of the phase difference on coherence in accordance with the Cramer–Rao boundary conditions from (Rodríguez and Martin, 1992) is as follows:

$$\sigma^2\left(\Delta\varphi\right) = \frac{1}{2N_L}\frac{1-\gamma^2}{\gamma^2}, \quad (3)$$

where N_L is the number of samples in the spatial ensemble. In accordance with this, a consequence of the decrease in coherence is an increase in the dispersion of the interferometric phase difference.

Under ideal conditions of a stable surface and negligible equipment noise, the main contribution to the phase difference in the interferogram φ, dependent on the difference in slant ranges, is introduced by the "topographic" phase φ_{topo}, transmitting variations in surface topography. In the general case, the value of the phase difference φ is influenced by, in addition to the relief, small-scale areal displacements of the surface (surface dynamics) during the time between surveys φ_d, atmospheric fluctuations in the electrical path length of the radar signal φ_a, fluctuations in the electrical path length of the radar signal φ_s in the snow-ice layer accumulating on the ground during the cold sea-

son, random shifts in the position of the phase scattering center due to spatial and temporal decorrelation φ_{spat} and φ_{temp}, receiving system noise (including ADC quantization noise) φ_n, noise introduced by the processing system φ_p, as well as the unknown initial phase difference φ_0, which is the same for the entire interferogram (Zakharov et al. 2015):

$$\Delta\varphi = \Delta\varphi_{topo} + \Delta\varphi_d + \Delta\varphi_a + \Delta\varphi_s + \Delta\varphi_{spat} + \Delta\varphi_{temp} + \Delta\varphi_n + \Delta\varphi_p + \Delta\varphi_0. \quad (4)$$

The noises of spatial and temporal decorrelation, as well as the thermal noises, determine the interpixel accuracy of measurements; they can be reduced by spatial filtering of the interferogram with an inevitable decrease in spatial resolution.

To process interferometric pairs of images, the method of classical differential interferometry is used, when the topographic phase φ_{topo} on the interferogram is estimated from the data of the external digital elevation model and subtracted. For this purpose, a publicly available digital elevation model GMTED (Global Multi-resolution Terrain Elevation Data) was used, which is available at https://www.usgs.gov/core-science-systems/eros/coastal-changes-and-impacts/gmted2010. To reduce the noise level and bring it to the same linear resolution in azimuth and range, an incoherent summation of four adjacent interferogram pixels was performed. Additionally, nonlinear filtering of the interferogram was performed using the Goldstein filter (Goldstein and Werner, 1998) with an effective window size of 5×5. Relatively large-scale phase fluctuations on atmospheric inhomogeneities, as well as an additive in the form of an unknown initial phase φ_0, can be estimated from the signal of a known stable nearby surface object and excluded from (4).

The phase noise level φ_t, due to temporal decorrelation depends on the interval between observations of the interferometric pair. Temporal decorrelation increases with increase in the interval between surveys, with a change in the roughness and dielectric properties of the scattering surface layer; therefore, when compiling interferometric pairs, it is preferable to use images with a small interval between surveys, taken under similar seasonal and meteorological conditions, as well as similar moisture contents.

By processing noise φ_p we usually understand the noise of calculations due to the finite number of bits in the digital representation of the signal; however, the use of Sentinel-1 data introduces its own characteristics. Due to the high steepness of the edges of the Doppler centroid in the elementary frame for the TOPS mode, errors in combining Sentinel-1 images from different observations lead to a noticeable phase shift over the frame field both in the azimuthal and transverse directions. Thus, according to estimates (Lanari et al., 2015), coregistration errors on the order of several thousandths of a pixel give a noticeable (by several degrees) phase shift at the edges of the frame. Therefore, image registration errors can be a source of uncontrolled phase errors in the interferograms.

The accuracy of phase measurements under surveying at middle and high latitudes is reduced due to a sharp change in the dielectric properties of the underlying covers and snowfall/melt in the cold season. In (Guneriussen et al., 2001), a simple relationship was established between the increment in one-way signal-path length (and phase) and the increment in snow-cover thickness during the time between surveys. However, it is impossible to obtain sufficiently accurate phase corrections based on data on the thickness of the fallen snow layer according to data from nearby ground-based weather stations due to local features of snowfall, snow transport by winds in open areas, as well as snow clearing/removal in the survey area.

The phase difference identified with some degree of accuracy $\Delta\varphi_d$ is associated with the change in the difference in slant ranges due to the displacement of the surface Δr_d in the time between observations by the following ratio:

$$\Delta\varphi_d = -4\pi\lambda^{-1}\Delta r_d. \quad (5)$$

It should be emphasized that a change by half a wavelength (2.8 cm for SAR Sentinel-1) in the one-sided length of the signal path during the time between taking of an interferometric pair of images leads to an additional phase shift of 2π, which does not permit this change to be revealed. We add that the appearance of a layer of fresh snow about 10.5 cm thick with the previously given physical parameters during the time between surveys also gives an additional phase shift of 2π, and is therefore also not revealed.

The first ideas about the presence or absence of the dynamics of the underlying surface on the territory of the TPP-3 according to processing of the Sentinel-1B interferometric data for the period May 10–June 3, 2020 (the accident occurred between these dates) were described in (Zakharov et al., 2020). On the interferogram (Fig. 3, left) halftones represent variations of the interferometric phase difference from 0 to 2π, which correspond to possible radial displacements of the surface in the range from 0 to 2.8 cm. On the right is the amplitude image corresponding to the interferogram, on which the echo signals of tanks No. 2–No. 5 are circled. Inside the circle, the interferogram shows the position of the phase-difference profile passing through all four reservoirs from northwest to southeast. The phase values along this profile would deviate from a constant value if the reservoirs were shifted, which could be caused by the melting of the frozen ground. To study the influence of other effects on the position of the reservoirs (for example, frost heaving in winter) besides permafrost thawing in the warm season, interferograms for the autumn–winter period of 2019–2020 were also analyzed. It turned out that rela-

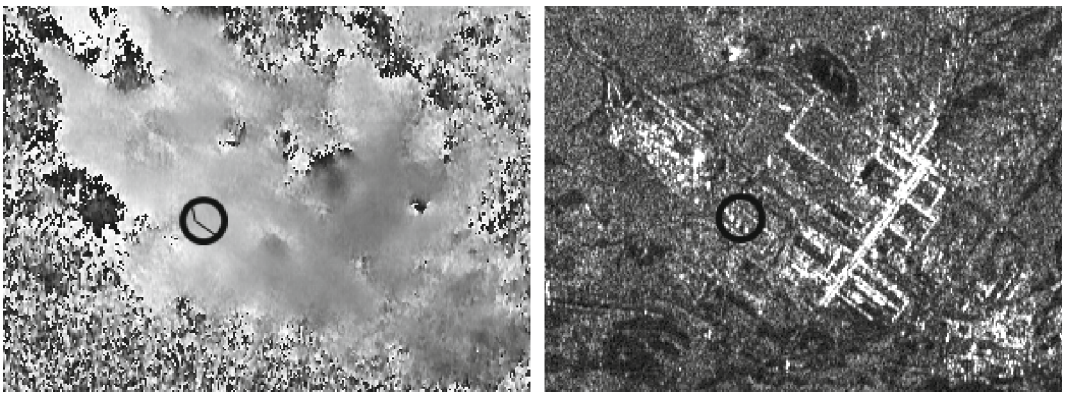

Fig. 3. Fragments of the interferogram (left) and Sentinel-1 amplitude image (right) for the interferometric pair May 10–June 3, 2020.

tive to the beginning of the profile, where the position of one supposedly stable reservoir was taken as a reference point, all fluctuations in the position of the remaining reservoirs, including the damaged one, are within 2–3 mm at all observation intervals. It was concluded that frost heaving in the winter of 2019–2020 and thawing of soils in the area of the TPP-3 in April–May 2020 did not lead to any noticeable displacement of the eastern walls of the reservoirs and the adjacent surface of the industrial site (Zakharov et al., 2020).

SHORT-TERM STABILITY ANALYSIS OF RESERVOIRS FROM JULY 2019 TO AUGUST 2020

Possible reasons for the damage to reservoir No. 5 could be earlier movements of the underlying surface, for which the time interval of interferometric observations must be extended, at the same time taking into account that a significant limiting factor in processing pairs of images with a large interval between surveys is the increase in temporal decorrelation. A generally accepted solution to the problem of monitoring slow surface motions under conditions of high temporal decorrelation is the use of the PS method (Ferretti et al., 1999) and similar methods. A feature of the PS method is the need to use long series of observations and the use of statistical analysis methods to identify reliable scatterers. The criterion for selecting candidate points for permanent scatterers is the stability of the signal scattering. An analysis of the scattering stability of the reservoirs over the interval from October 2017 to July 2020 showed that they do not meet the stability criterion from (Ferretti et al., 1999, 2000; Colesanti et al., 2003a, 2003b). The ratio of the standard deviation of the signal amplitude to the mean value in a series of 40 images is 0.6 for tank No. 2, 0.93 for No. 3, 0.81 for No. 4, and 0.98 for No. 5. The reason for such a high instability may be the influence of atmospheric precipitation, as well as the processes of melting/freezing of snow, on the characteristics of double bounce signal scattering by the large structures made up of the tank wall and the adjacent surface of the industrial site. The inevitable abrupt changes in the phase of the scattered signals due to changes in the radiophysical properties of the underlying covers differ from the slow monotonic changes assumed in the PS method, and therefore the PS family methods are not able to reliably identify reservoirs as permanent scatterers in this case, and thus they cannot be considered a reliable tool for measuring possible reservoir displacements. For this reason, in what follows, first of all, measurements made using a series of classical differential interferograms will be discussed, and phase measurements and further estimates of the dynamics of the reservoirs will be performed at the reservoir locations for which the maximum backscatter level is recorded.

To analyze the stability of the territory of the TPP-3 in the period from July 2019 to August 2020, presumably covering the main processes of displacement of the scattering objects, differential interferograms were constructed with 12-day intervals between surveys. Three objects were selected as a reference, presumably stable details on the scattering surface: a pipeline above the road (500 m northeast of the tanks), a triangular corner formed by a right angle of the building and the surface of the industrial site (1050 m in the east-southeast direction), and an element at the inner side of the fence around the tank area (70 m southwest of the scattering wall of tank No. 3). Google Earth images of these objects are shown in Fig. 4, where the arrows show their location. Within the burst image of Sentinel-1, the first two are the most stable point objects, with a high level of interferometric coherence, probably due to the small (compared to reservoirs) geometric dimensions of these objects. The coherence level of the signals from these objects exceeds 0.95 in all pairs of images taken from July 2019 to August 2020, except for the pairs containing September images, when the coherence decreased to 0.85, and the April images, with a coherence of 0.7. As can be

Fig. 4. Google Earth images containing reference objects: pipeline (left), inside corner of building (center), and construction at the tank fence (right).

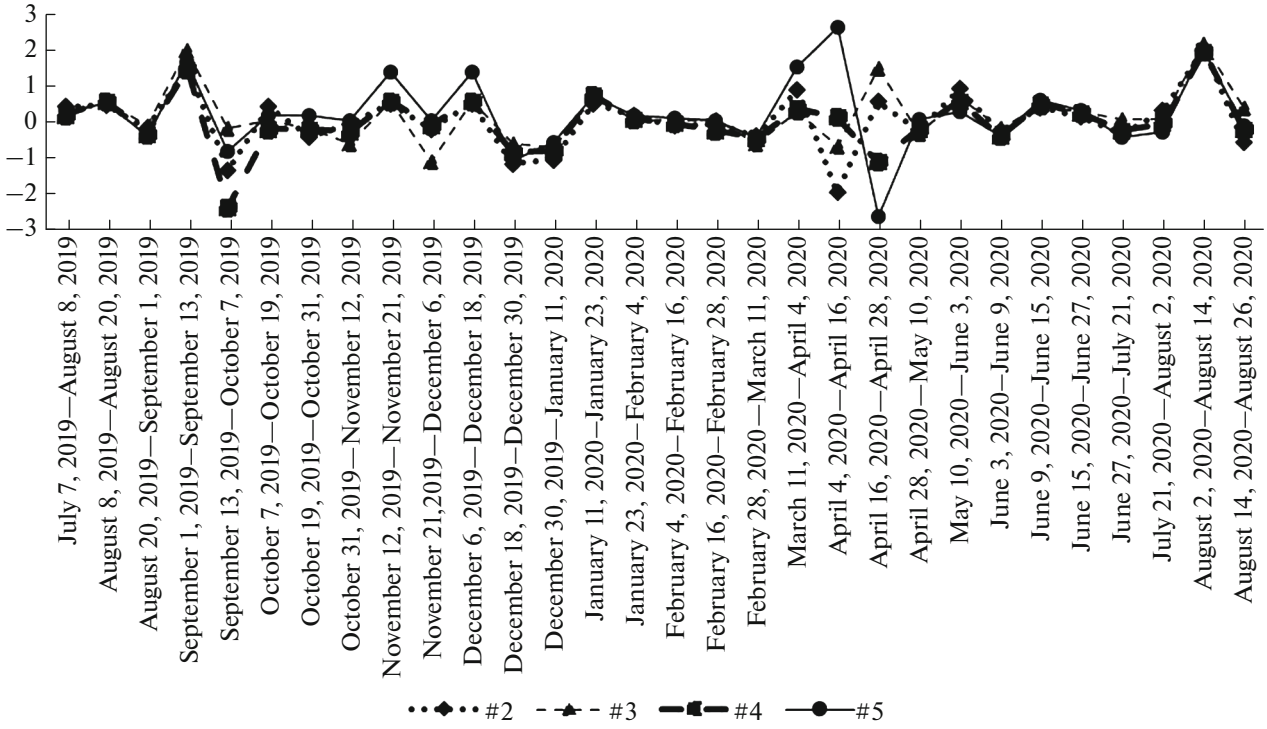

Fig. 5. The time course of the phase shifts of the tank signal relative to the pipeline (in radians), in the period from July 27, 2020 to August 8, 2020.

judged from some winter interferograms, a feature of the first of them, the pipeline above the road, is a single scattering of the radar signal by the pipe structure, usually not covered with a snow layer. The building as a corner reflector is characterized by consistent backscatter from two walls of the technical building and the adjacent surface of the industrial site. In this case, the effect of a layer of snow lying on the site is possible. Since this object had the highest coherence of backscatter in all interferograms, it was chosen as the reference one.

Figure 5 shows the time course of phase differences for four tanks No. 2–No. 5 at 12-day intervals from July 2019 to August 2020.

This figure shows the high stability (recurrence of graphs) of the phase difference of the fuel tanks for 12-day intervals of observing the dynamics relative to the reference object and relative to each other in the summer of 2019 and in December–March and May–August 2020 (small deviations from zero according to the chart). The phase deviations for the reservoirs in May–August are 0.2–0.3 rad, which corresponds to their possible mutual displacements in the direction of the satellite by 0.9–1.3 mm.

Figure 6 shows information about the average daily temperature and snow depth at the Norilsk meteorological station according to the webarchive www.rp5.ru.

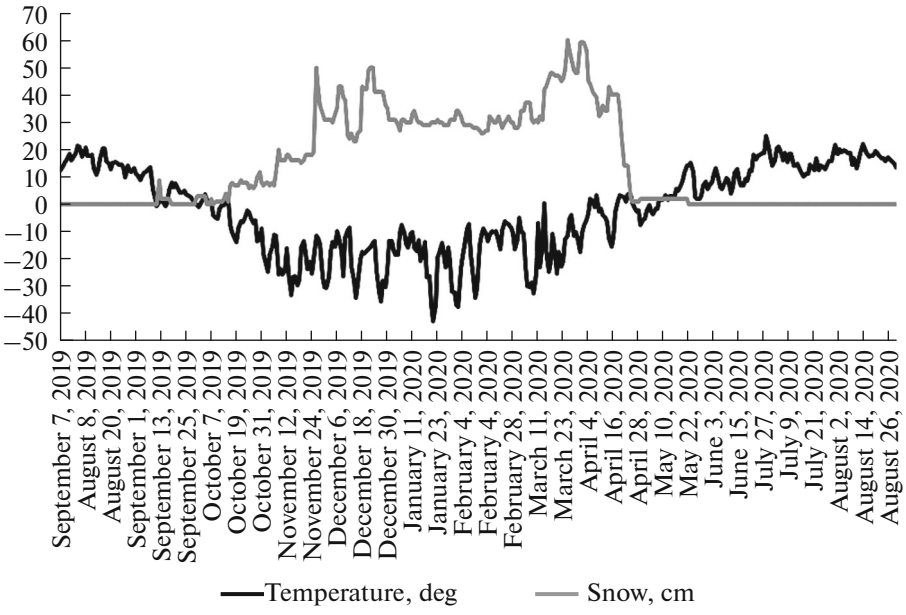

Fig. 6. Average daily air temperature and snow-cover thickness.

Note the influence of variations in the dielectric properties of the scattering covers as a result of snowfall on September 13 and from October 2019 to January 2020, as well as the melting/freezing of snow and ice covers in April 2020, on the strong increase in fluctuations in the phases of the reservoir signals over this time. Note that due to the 2π ambiguity of the phase measurements, errors are possible, leading to an underestimation of the real phase fluctuations and the corresponding signal-path length.

The transition of the average daily air temperature through zero in April and the intense snowmelt caused by this also caused an increase in fluctuations in the position of the phase scattering center by the dihedral corners of the tanks and an increase in the scatter of the phase measurements. Similarly, snowfall in autumn, modification of the snow-cover thickness by wind, and snow removal on the territory of the industrial zone, caused random changes in the snow-cover thickness near the reservoirs and an increase in phase fluctuations (see the left part of Fig. 6). The drop in the coherence of the reservoir signals from an average of 0.92 to 0.7–0.8 in autumn and early winter, as well as to 0.6–0.7 in April, is a good indicator of the reason for the sharp increase in phase fluctuations. At the same time, it can be argued that measurements of the phase of the signals scattered by the tanks indicate a high (about 1.3 mm) stability of the mutual position of the tanks and the surface of the industrial site in May–August 2020 at short, 12-day intervals, subject to high interferometric coherence.

A theoretical estimate of the accuracy of the interferometric measurements in the accepted processing technique can be obtained based on the level of coherence of the signals scattered by the reservoirs. The above formula (2) gives fairly accurate estimates of the phase errors under the condition of a high level of coherence. Having accepted $\gamma = 0.9$, we get the standard deviation of the phase equal to 0.34 radians. The corresponding measurement error for radial displacements does not exceed 1.5 mm, which corresponds to the experimental estimates made above.

It is necessary to comment separately on the phase measurements for tank No. 5, the dismantling of which began at the end of July 2020: despite the absence of a double bounce backscatter signal, in the phase of the signal S_S, scattered by the surface of the industrial site at the location of the reservoir, one can judge the remaining stability of the position of the underlying surface during the dismantling of the reservoir, and afterwards, in August 2020.

ANALYSIS OF THE STABILITY OF THE POSITION OF RESERVOIRS AT ANNUAL INTERVALS

To detect monotonous slow displacements of the underlying covers over long time intervals, it is most appropriate to carry out measurements on a series of differential interferograms with an increasing time interval between surveys and a single base survey session. We chose the image taken on September 1 as a starting point, it was the last one held in warm, dry weather in early autumn. The phase measurements for reservoir No. 5 based on 23 interferograms in the period from September 1, 2019 to July 21, 2020 are given in Fig. 7 as a solid line. The dates of the second image in the interferometric pair are plotted along the abscissa

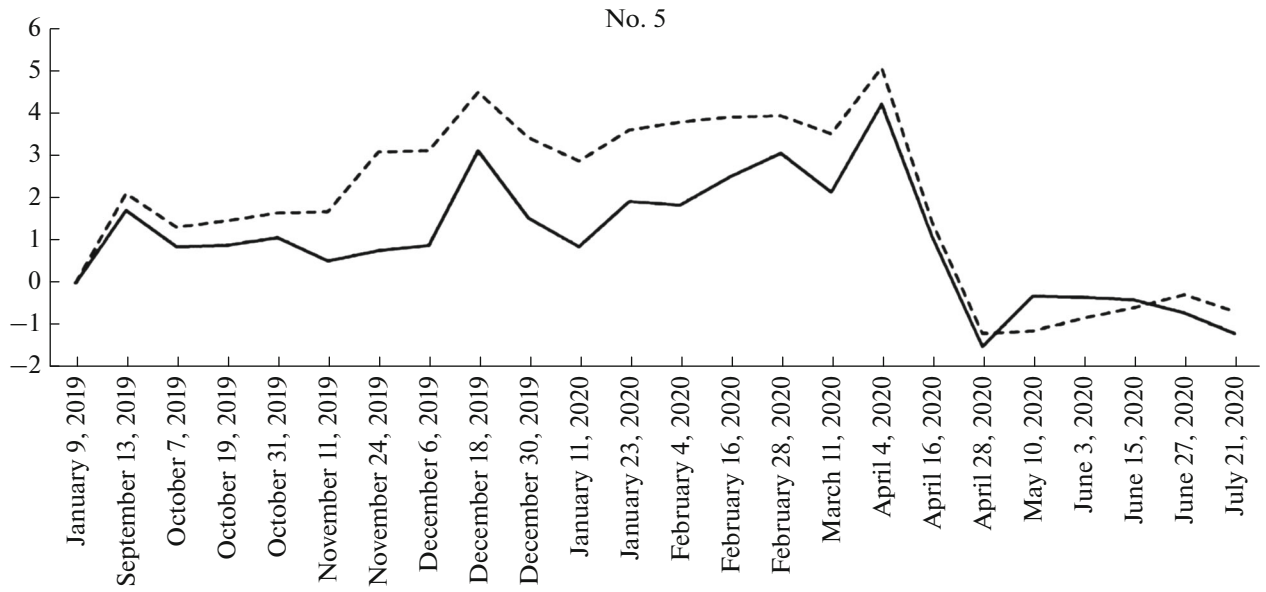

Fig. 7. Growth of the phase differences of the signals of reservoir No. 5 (in radians) over a one-year time interval with an increase in the time interval between surveys (solid line) and accumulation of measurements of short intervals (dashed line).

axis. A feature of such interferograms with long intervals is the decrease in coherence to 0.6–0.7 near the reservoirs in winter due to the increase in the temporal decorrelation of backscatter and the inevitable decrease in phase measurement accuracy.

For comparison, let us form a similar graph by summing with the accumulation of phase differences over short intervals with Fig. 5 for tank No. 5. A feature of this version of the phase measurements is the accumulation of measurement errors over short intervals, although with a higher accuracy of individual measurements (higher interferometric coherence due to shorter time intervals).

In Fig. 7, the dotted line shows the result of such accumulation over a one-year time interval starting from September 1, 2019. The end point of the accumulation interval is plotted along the abscissa.

The phase graphs that almost coincide at the beginning of the interval diverge in the cold season by about 2 radians due to an increase in measurement errors under conditions of reduced coherence of the signals from the interferometric pairs. We note a steady increase in the phase difference from October to March, which is most likely due to the accumulation of snow as a result of snowfall and wind transport of snow. The difference in measurements decreases after the snow cover melts in April. Starting from May, the phase values are close to –0.5 rad, which is close to the measurement error, although it can be interpreted as a shift of the tank's effective phase scattering center by 2 mm upwards. It can be argued that the winter increase in the phase differences is the result of snow accumulation near the reservoir, and not of the monotonous subsidence, which ended in April with the return of the scattering object to its original position.

To check the reliability of the near-zero values of the phases after the melting of the snow cover, 18 pairs of images were processed with long, more than half-year, intervals between surveys, obtained exclusively in the warm season and containing the winter period within the interval. When choosing reliable phase measurements, we excluded measurements that were accompanied by a coherence below 0.8. Summer surveys were excluded that were characterized by precipitation on the day of the survey or total precipitation of more than 4 mm in the five days before one of the surveys. Figure 8 shows phase measurements for four reservoirs on 10 interferometric pairs with long, from 6 to 12 months, intervals between surveys in the period from July 2019 to July 2020.

Based on the given coherence-level requirements, tanks No. 2 and No. 5 had three measurements each

Table 1. Phase measurements over reservoirs on annual interferograms, rad

Shooting dates	Tank #2	Tank #3	Tank #4	Tank #5
July 25, 2017–July 20, 2018	0.1	0.1	0.6	0.5
July 20, 2018–July 27, 2019	–0.9	–0.7	–1.2	–0.9
July 27, 2019–May 10, 2020	0.8	–1.6	–1.1	0.4

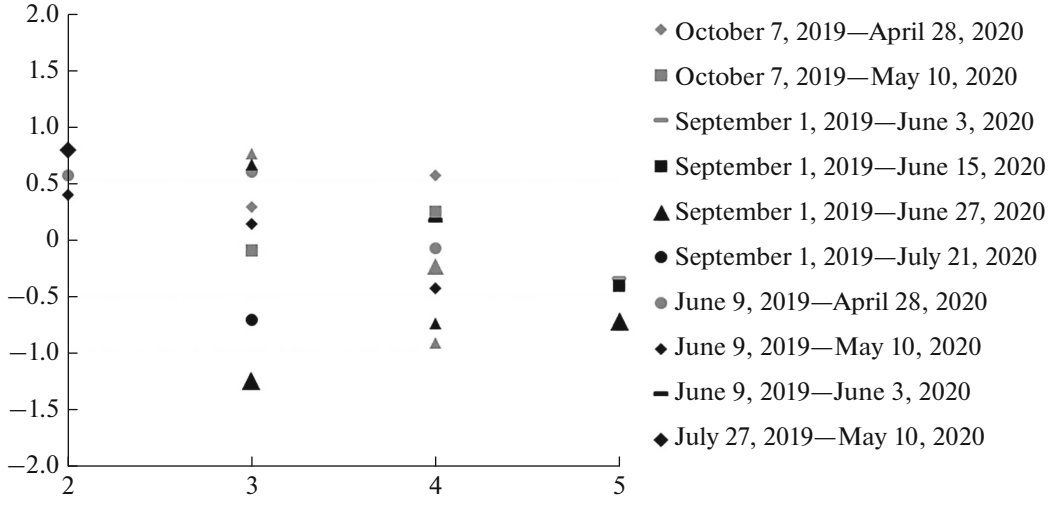

Fig. 8. Phase measurements for reservoirs with long time intervals between surveys.

and tanks No. 3 and No. 4 had eight measurements each. The phase average is 0.6 rad for reservoir No. 2, 0.06 rad for No. 3, –0.17 rad for No. 4, and –0.49 rad for No. 5. It can be seen that the mutual position of the reservoirs in phase is within 1 rad, which is equivalent to a potential mutual shift of 0.4 cm along the slant range.

A similar level of stability of the mutual position of the reservoirs at annual intervals was also observed several years earlier, in the processing of the Sentinel-1 SAR data obtained in the period 2017–2019. Three sets of phase measurements for the fuel tanks on the summer interferograms with a one-year interval are given in Table 1. The condition for selecting these pairs of images was the absence of significant precipitation on the day of the survey, as well as in the few days before the survey.

Despite the revealed increased scattering instability at short survey intervals in autumn and spring within the cold season of 2019–2020, the measurements from Table 1 indicate a rather high stability of the position of the scattering centers of the reservoirs at annual intervals in 2017–2019. The standard deviation of the phase fluctuations in each interferogram is within 0.7–1 rad, which corresponds to object position fluctuations within 4.5 mm. These results allow us to make an assumption about the stability of the position of the fuel tanks of the TPP-3 and the adjacent areas of the industrial site. At the same time, it must be remembered that the relatively low, worse than 10 m, spatial resolution of the used radar data does not make it possible to identify possible areal displacements of surface areas of a smaller linear size, which may have caused the damage to the tank No. 5.

CONCLUSIONS

The use of radar interferometry methods for monitoring the stability of the fuel tanks at TPP-3 in order to clarify the cause of the accident at the tank No. 5, which resulted in the leakage of a large volume of diesel fuel into the environment, is greatly complicated by the distorting effect of precipitation: snow buildup in the cold season and its melting in spring. A feature of the signal backscattering by the tank is the double bounce of the signal sequentially by its side wall and the adjacent area of the TPP-3 industrial site. Wetting/drying of the surface of the adjacent site and the accumulation of snow cover on it in winter and its melting in spring lead to changes in the scattering properties of this face of the dihedral angle, shifts in the position of the scattering phase centers, and errors in interferometric measurements of the phase difference of the signals of repeated surveys. The results of the study of variations in the interferometric phase difference at the locations of the reservoirs allow us to conclude that the mutual position of all four TPP reservoirs (their eastern walls) and the territory adjacent to them was stable in the range of 2–3 mm when measured at 12-day time intervals in autumn 2019–summer 2020, including the 24-day time interval covering the emergency event. In the warm time of the observation interval of this period, the mutual stability of the positions of the reservoirs was within 1.3 mm. At one-year time intervals between surveys, fluctuations in the position of the reservoirs do not exceed 4.5 mm, including in 2017–2018 and 2018–2019. It can be assumed that the depressurization of the reservoir was not caused by areal displacements of the scattering surfaces and structures on the territory of TPP-3, at least since July 2017.

FUNDING

The work was carried out within the framework of the state assignment.

REFERENCES

Bamler, R. and Hartl, P., Synthetic aperture radar interferometry, *Inverse Probl.*, 1998, vol. 14, pp. R1–R54.

Berardino, P., Fornaro, G., Lanari, R., and Sansosti, E., A new algorithm for surface deformation monitoring based on small baseline differential SAR interferograms, *IEEE Trans. Geosci. Remote Sens.*, 2002, vol. 40, no. 11, pp. 2375–2383.

Bondur, V.G., Aerospace methods and technologies for monitoring oil and gas areas and facilities, *Izv., Atmos. Ocean. Phys.*, 2011, vol. 47, no. 9, pp. 1007–1018.

Bondur, V.G. and Starchenkov, S.A., Methods and programs for processing and classification of aerospace images, *Izv. Vyssh. Uchebn. Zaved., Geod. Aerofotos'emka*, 2001, no. 3, pp. 118–143.

Colesanti, C., Ferretti, A., Novali, F., Prati, C., and Rocca, F., SAR monitoring of progressive and seasonal ground deformation using the permanent scatterers technique, *IEEE Trans. Geosci. Remote Sens.*, 2003a, vol. 41, pp. 1685–1700.

Colesanti, C., Ferretti, A., Prati, C., and Rocca, F., Monitoring landslides and tectonic motion with the permanent scatterers technique, *Eng. Geol.*, 2003b, vol. 68, pp. 3–14.

Dagurov, P.N., Dmitriev, A.V., Dobrynin, S.I., Zakharov, A.I., and Chimitdorzhiev, T.N., Radar interferometry of the soil's seasonal deformations and the phase model of backscattering of microwaves by a two-layer medium with rough boundaries, *Opt. Atmos. Okeana*, 2016, vol. 29, no. 7, pp. 585–591.

Ferretti, A., Prati, C., and Rocca, F., Permanent scatterers in SAR interferometry, in *Proc. of the IEEE International Geoscience and Remote Sensing Symposium (IGARSS-1999)*, Hamburg, Germany, 1999, vol. 3, pp. 1528–1530.

Ferretti, A., Prati, C., and Rocca, F., Nonlinear subsidence rate estimation using permanent scatterers in differential SAR interferometry, *IEEE Trans. Geosci. Remote Sens.*, 2000, vol. 38, no. 5, pp. 2202–2212.

Ferretti, A., Fumagalli, A., Novali, F., Prati, C., Rocca, F., and Rucci, A., A new algorithm for processing interferometric data-stacks: SqueeSAR, *IEEE Trans. Geosci. Remote Sens.*, 2011, vol. 49, no. 9, pp. 3460–3470.

Goldstein, R.M. and Werner, C.L., Radar interferogram filtering for geophysical applications, *Geophys. Res. Lett.*, 1998, vol. 25, no. 21, pp. 4035–4038.

Guneriussen, T., Hogda, K.A., Johnsen, H., and Lauknes, I., InSAR for estimation of changes in snow water equivalent of dry snow, *IEEE Trans. Geosci. Remote Sens.*, 2001, vol. 39, no. 10, pp. 2101–2108.

Hooper, A., Zebker, H., Segall, P., and Kampes, B., A new method for measuring deformation on volcanoes and other natural terrains using InSAR persistent scatterers, *Geophys. Res. Lett.*, 2004, vol. 31, no. 23, L23611. https://doi.org/10.1029/2004GL021737

Kobak, V.O., *Radiolokatsionnye otrazhateli* (Radar Reflectors), Moscow: Sov. Radio, 1975.

Lanari, R., Berardino, P., Bonano, M., Casu, F., De Luca, C., Elefante, S., Fusco, A., Manunta, M., Manzo, M., and Ojha, C., Sentinel-1 results: SBAS-DInSAR processing chain developments and land subsidence analysis, in *IEEE Int. Geosci. Remote Sens. Symp. (IGARSS-2015)*, 2015, pp. 2836–2839.

Rodríguez, E. and Martin, J.M., Theory and design of interferometric synthetic-aperture radars, *Proc. IEEE*, 1992, vol. 139, no. 2, pp. 147–159.

Rosen, P.A., Hensley, S., Joughin, I.R., Li, F.K., Madsen, S.N., Rodriguez, E., and Goldstein, R.M., Synthetic aperture radar interferometry, *Proc. IEEE*, 2000, vol. 88, no. 3, pp. 333–392.

Torres, R., Snoeij, P., Geudtner, D., Bibby, D., Davidson, M., Attema, E., Potin, P., Rommen, B., Floury, N., Brown, M., Navas Traver, I., Deghaye, P., Duesmann, B., Rosich, B., Miranda, N., et al., GMES Sentinel-1 mission, *Remote Sens. Environ.*, 2012, vol. 120, pp. 9–24.

Vasil'evskaya, V.D., *Pochvoobrazovanie v tundrakh Srednei Sibiri* (Soil Formation in Middle Siberian Tundras), Moscow: Nauka, 1980.

Zakharov, A.I. and Zakharova, L.N., Observation of snow cover dynamics on L-band SAR interferograms, *Sovrem. Probl. Distantsionnogo Zondirovaniya Zemli Kosmosa*, 2017, vol. 14, no. 7, pp. 190–197.

Zakharova, L.N. and Zakharov, A.I., Detection of bridges instability by means of SAR interferometry, *Sovrem. Probl. Distantsionnogo Zondirovaniya Zemli Kosmosa*, 2018, vol. 15, no. 2, pp. 42–51.

Zakharova, L.N. and Zakharov, A.I., Interferometric observation of landslide area dynamics on the Bureya River by means of Sentinel-1 radar data in 2017–2018, *Sovrem. Probl. Distantsionnogo Zondirovaniya Zemli Kosmosa*, 2019, vol. 16, no. 2, pp. 273–277.

Zakharov, A.I., Yakovlev, O.I., and Smirnov, V.M., *Sputnikovyi monitoring Zemli: Radiolokatsionnoe zondirovanie poverkhnosti* (Earth Satellite Monitoring: Radar Sensing of the Surface), Moscow: URSS, 2015.

Zakharov, A.I., Zakharova, L.N., and Krasnogorskii, M.G., Monitoring landslide activity by radar interferometry using trihedral corner reflectors, *Izv., Atmos. Ocean. Phys.*, 2018, vol. 54, no. 9, pp. 1110–1120.

Zakharov, A.I., Zakharova, L.N., and Mitnik, L.M., Monitoring of the Norilsk TPP-3 fuel tanks stability by means of radar interferometry technique, *Sovrem. Probl. Distantsionnogo Zondirovaniya Zemli Kosmosa*, 2020, vol. 17, no. 5, pp. 281–285.